Topographically Induced Changes in the Structure of an Inertial Coastal Jet: Application to the Agulhas Current

A. E. GILL

Department of Applied Mathematics and Theoretical Physics, University of Cambridge, England

E. H. SCHUMANN

National Research Institute for Oceanology, Congella, South Africa

(Manuscript received 9 May 1978, in final form 7 February 1979)

ABSTRACT

Calculations are made of the changes in the structure of an inertial current which can be induced by slow changes in the topography of the continental shelf and slope along which it flows. The particular case of a uniform potential vorticity current over a shelf of uniform slope shows that smooth transitions from subcritical to supercritical flow can occur at a minimum in the shelf width. Long-wave disturbances travel away from such a point. Upstream there is a tendency for a countercurrent to occur at the coast, while downstream there is a tendency for cold water to outcrop on the inshore side of a front. Both these features occur along the path of the Agulhas Current.

A method developed for calculating the speed of long-wave disturbances in a flow with a given potential vorticity distribution is applied to sections of the Agulhas Current about 150 km apart. In this distance the shelf width is reduced, and a calculation using a current model with two active layers shows the second mode is very close to critical at Port Edward. This result supports the notion that shelf topography can hydraulically control an inertial boundary current.

1. Introduction

The situations to be considered in this paper involve the flow of an inertial jet along a coastal boundary, with the basic premise being the conservation of potential vorticity in various layers as the current moves into different regimes. Thus, changes in both the local vertical component of the Coriolis parameter f and topographic changes can alter the nature of the jet.

Of course such a concept is not new, but has been used previously in two different kinds of ways to study the behavior of intense narrow current systems such as the Gulf Stream. One, which is not adopted here, concentrates on the *path* of the jet and has been used, for instance, to explain the meandering of the Gulf Stream (e.g., Warren 1963; Niiler and Robinson, 1967).

The approach followed here concentrates on the structure of the inertial current, where its path is well defined because it is constrained to follow a boundary. This approach is exemplified in Stommel (1960, Chap. 8, hereafter referred to as Stommel), where the theories of Morgan (1956) and Charney (1955) are also discussed. These latter two authors attempted to find a boundary current which could be produced by a specified inflow. It was argued that this inflow would be determined by the Sverdrup solution for the main part of the ocean gyre. Each parcel of water entering the boundary current has a predetermined potential vorticity, and the combined effect of many parcels of different origins then determines the structure of the stream.

In practice the potential vorticity of a fluid parcel changes due to friction and mixing effects, so modeling by an ideal fluid can only be applied over limited path lengths. In studying the variability of western boundary currents, Niiler (1975) mentions that vorticity tends to be conserved between two sections across the Gulf Stream. Here the object is to model changes in the structure of the Agulhas Current caused by fairly large changes in shelf topography over distances of the order of a few hundred kilometers, so it is hoped that neglect of friction effects is reasonable in these circumstances.

In all models considered, the f-plane approximation will be made, i.e., the Coriolis parameter will be assumed constant over a given section. Since these tend to be nearly parallel to lines of latitude, little error can be introduced here; changes in f are readily accommodated when moving to a new section.

The solutions for current structure are particularly simple when the potential vorticity in a layer is uniform, so modeling begins with cases which have

0022-3670/79/050975-17$08.25
© 1979 American Meteorological Society

this property. Stommel in fact argued that "the potential vorticity in the upper layers of the Gulf Stream is fairly uniform across the Stream", and showed that the velocity profile could in large measure be ascribed to the narrowing of a vertical layer of constant potential vorticity water across the flow of the Stream. The initial models treated thus have only one layer with uniform potential vorticity lying above an inactive lower layer. Nonetheless, with a variable shelf topography, results are obtained which indicate that subcritical and supercritical flow can occur around a control section where there is a minimum shelf width. Long-wave disturbances travel away from such a point, and associated countercurrents and upwelling may occur in practice where similar phenomena have been observed in the Agulhas Current.

In later sections a multi-layer model with variable potential vorticities is developed, and the structural changes undergone by the Agulhas Current when moving between two test sections simulated with some degree of success. It also proves possible to determine the speed of two baroclinic modes of the long waves propagating in the system, with the results supporting the general conclusions reached with the simpler models.

2. Equations

We suppose the system to be studied consists of a narrow boundary current flowing along a straight coastline. A right-handed co-ordinate system (x,y,z) is chosen to specify position, with the x axis pointing seaward, the y axis parallel to the coast and the z axis vertically upward. The Boussinesq and hydrostatic approximations will be made, and the width of the current will be assumed small compared with the scale of longshore variations. (The last assumption means that the coast need not be perfectly straight but can bend slowly on a scale which is large compared with the width of the current without altering the equations to first order.) Stratification effects are incorporated by supposing the ocean to be divided into a set of superposed layers each of uniform density ρ_i, where the index i starts with 1 in the upper layer, and increases downward. The depth of layer i at a given (x,y,t) will be denoted D_i and the horizontal velocity (u_i,v_i). This velocity will be assumed to be uniform over the depth.

We first consider the hydrostatic equation for pressure p. Integrating downward from $z = 0$, and requiring continuity at each interface $z = -D_1$, $z = -D_1 - D_2$, etc., gives for a point in layer n,

$$p = p(0) - \rho_n g z + \sum_{i=1}^{n} (\rho_i - \rho_n) g D_i. \quad (2.1)$$

Here g is the acceleration due to gravity, and $p(0)$ is the pressure due to variations in the surface elevation (the effect of atmospheric pressure being neglected here). Now pressure appears in the momentum equations only in the form of horizontal gradients, i.e., in terms such as

$$\frac{1}{\rho_n}\frac{\partial p}{\partial x} \equiv \frac{\partial p_n}{\partial x},$$

$$p_n = \frac{p(0)}{\rho_n} + \sum_{i=1}^{n} \left(\frac{\rho_i - \rho_n}{\rho_n}\right) g D_i. \quad (2.2)$$

Hence the term in (2.1) involving z is not needed. In fact, the $p(0)$ term is not needed either since subsequent analysis requires only knowledge of the differences between p_n's, for which (2.2) gives, after use of the Boussinesq approximation

$$p_{n+1} - p_n = -g_n \sum_{i=1}^{n} D_i, \quad (2.3)$$

where

$$g_n = g(\rho_{n+1} - \rho_n)/\rho_n \quad (2.4)$$

is the reduced gravity between layers n and $n + 1$.

In addition to the set of equations (2.3), there are three equations for each layer, *viz.*, the two horizontal components of the momentum equation and the continuity equation. Because of the scale assumptions a quasi-geostrophic situation exists, i.e., the longshore component of velocity is in geostrophic balance with the offshore pressure gradient, and so for layer i the equations are

$$f v_i = -\frac{\partial p_i}{\partial x}, \quad (2.5)$$

$$\frac{\partial v_i}{\partial t} + u_i\frac{\partial v_i}{\partial x} + v_i\frac{\partial v_i}{\partial y} + f u_i = -\frac{\partial p_i}{\partial y}, \quad (2.6)$$

$$\frac{\partial D_i}{\partial t} + u_i\frac{\partial D_i}{\partial x} + v_i\frac{\partial D_i}{\partial y} + D_i\left(\frac{\partial u_i}{\partial x} + \frac{\partial v_i}{\partial y}\right) = 0. \quad (2.7)$$

It often proves useful to replace (2.6) and (2.7) by two equations which can be derived from them. The first of these is the potential vorticity equation which is obtained by subtracting $(f + \partial v_i/\partial x)/D_i^2$ times (2.7) from D_i^{-1} times the x derivative of (2.6). This gives

$$\left(\frac{\partial}{\partial t} + u_i\frac{\partial}{\partial x} + v_i\frac{\partial}{\partial y}\right)\left(\frac{f + \partial v_i/\partial x}{D_i}\right) = 0 \quad (2.8)$$

and expresses the conservation of potential vorticity $(f + \partial v_i/\partial x)/D_i$ by a particle moving with the fluid. Since f is assumed constant, the "potential depth" $\bar{D}_i$, defined by

$$\frac{f + \partial v_i/\partial x}{D_i} = \frac{f}{\bar{D}_i}, \quad (2.9)$$

is also conserved for a material particle.

The second of the two derived equations is merely a rearrangement of (2.6), *viz.*,

$$\frac{\partial v_i}{\partial t} + \left(f + \frac{\partial v_i}{\partial x}\right)u_i = -\frac{\partial B_i}{\partial y}, \tag{2.10}$$

where

$$B_i = p_i + \tfrac{1}{2}v_i^2 \tag{2.11}$$

is the Bernoulli function for the layer (since $v_i \gg u_i$). The above manipulations are fairly standard and are given for a single layer by Stommel. Note that if (2.9) is used in (2.10), it can be written as

$$-D_i u_i = \frac{\bar{D}_i}{f}\left(\frac{\partial v_i}{\partial t} + \frac{\partial B_i}{\partial y}\right) \equiv \frac{\bar{D}_i}{f}\left(\frac{\partial v_i}{\partial t} + v_i\frac{\partial v_i}{\partial y} + \frac{\partial p_i}{\partial y}\right) \tag{2.12}$$

and regarded as an equation for the onshore transport $-D_i u_i$ in the ith layer.

3. A two-layer model without topography

The first model to be considered is that of a homogeneous layer of uniform potential vorticity overlying a very deep bottom layer. The approach for a steady system follows that of Stommel, who found that it gives a reasonable representation of a section across the Gulf Stream. Here the model is also applied for a time-varying boundary current adjacent to a straight vertical boundary, and is similar to a model of Bennett (1973) for large-amplitude Kelvin waves. In the next sections, this model will be modified by having a sloping boundary region, so that topographic effects can be considered.

The bottom layer ($i = 2$) is supposed to be so deep that currents in it (but not necessarily transports) are effectively zero and hence pressure gradients are zero. Thus p_2 may be taken zero, and so (2.3) with $n = 1$ gives

$$p_1 = g_1 D_1. \tag{3.1}$$

Since only layer 1 is active, there is no need for subscripts and these will be dropped (subscript 1 is implied when none is given).

Now using the potential vorticity equation (2.9), the geostrophic balance equation (2.5), and (3.1) to eliminate p and v for this layer gives

$$\frac{\partial^2 D}{\partial x^2} = \frac{D - \bar{D}}{a^2}, \tag{3.2}$$

where a (a positive number) is the Rossby radius of deformation defined by

$$a^2 = \frac{g_1 \bar{D}}{f^2}. \tag{3.3}$$

Note that a depends on the potential depth $\bar{D}$ (a constant here), rather than on any local depth which might be considered typical of the current.

It is convenient to write these equations in a nondimensional form using $\bar{D}$ as the unit of depth, a as the unit of horizontal distance and af as the unit of velocity. If an asterisk is used temporarily to denote the nondimensional quantities, the definitions are

$$\left.\begin{aligned} &D^* = D/\bar{D}, \quad t^* = ft, \quad p^* = p/g_1\bar{D} \\ &(x^*,y^*) = (x,y)/a, \quad (u^*,v^*) = (u,v)/af \end{aligned}\right\}. \tag{3.4}$$

If the asterisks are now dropped, the nondimensional form of the equations is

$$\left.\begin{aligned} p &= D \\ 1 + \frac{\partial v}{\partial x} &= D \\ v &= \frac{\partial p}{\partial x} \\ \frac{\partial^2 D}{\partial x^2} &= D - 1 \\ -Du &= \frac{\partial v}{\partial t} + v\frac{\partial v}{\partial y} + \frac{\partial p}{\partial y} \end{aligned}\right\}, \tag{3.5}$$

with a solution

$$p = D = 1 + (\Delta - 1)e^{-x}, \tag{3.6}$$

$$v = (1 - \Delta)e^{-x}, \tag{3.7}$$

where Δ is defined as the value of D at the vertical boundary at $x = 0$. This solution was used by Stommel as a model of the Gulf Stream. It can also be used (cf. Bennett 1973) to model time-dependent currents because Δ can vary with y and t.

The equation for Δ comes from applying the last of (3.5) at $x = 0$ where u vanishes, with the result

$$\frac{\partial \Delta}{\partial t} - \Delta\frac{\partial \Delta}{\partial y} = 0, \tag{3.8}$$

For small perturbations (for which Δ is close to unity), this represents a Kelvin wave moving at unit speed in the $-y$ direction, i.e., equatorward at a western boundary and poleward at an eastern boundary. For large perturbations, waves still move in this direction, but at a speed Δ which depends on the amplitude. In dimensional terms this speed is

$$c = -af\frac{\Delta}{\bar{D}} = -\left(\frac{g_1}{\bar{D}}\right)^{1/2}\Delta. \tag{3.9}$$

Note that the speed drops to zero as $\Delta \to 0$. When $\Delta = 0$, the coastal boundary is irrelevant and the line where the interface breaks the surface represents a front. Since $c = 0$, distortions of such a uni-

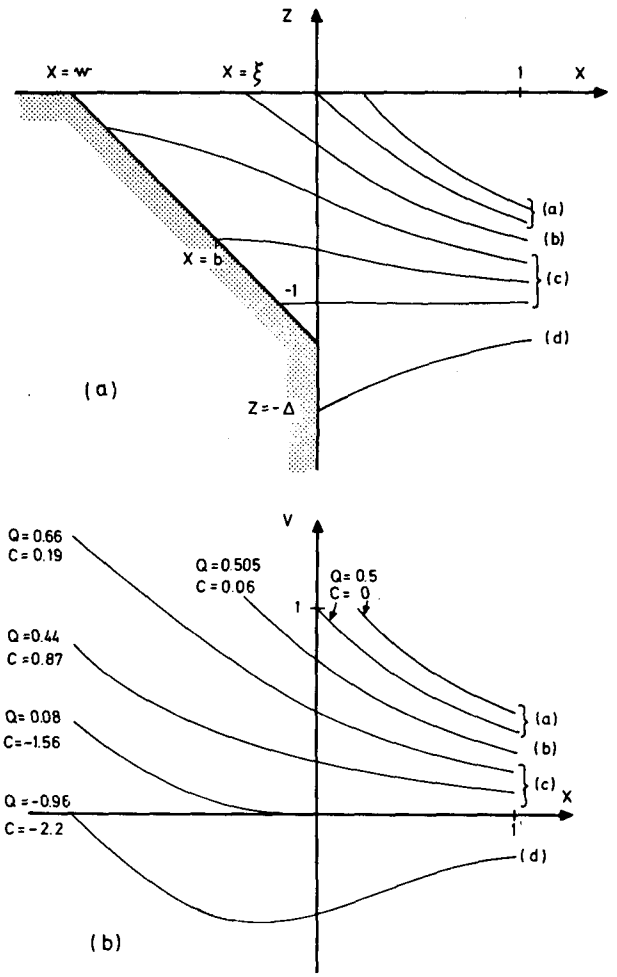

FIG. 1a. Geometry of the model designed to show the effects of shelf topography on an inertial boundary current. The four different positions of the interface treated in the text are shown; initially an arbitrary shelf profile is considered, but the drawing here is for the special case of a linear shelf with unit slope (in nondimensional units) and a width of 1.2.

FIG. 1b. Velocity profiles for the upper layer for the special case shown in 1a. Values are given in nondimensional units. On each curve, the total flux Q for the upper layer is given, and also the speed c of long-wave disturbances.

form potential vorticity front do not propagate but remain stationary.

4. Effects of variable topography: Cases with an offshore front

The aim of these next two sections is to include a variable shelf topography into the simple two-layer model of the previous section and to examine its effect on the inertial current. This more realistic geometry is illustrated in Fig. 1. The region $x > 0$ has a deep lower layer so as to retain the features already developed, but the shelf topography for $x < 0$ is arbitrary with the depth given by $H = H(x,y)$. The coast is at $x = w$ (where w is negative) and details are complicated somewhat by the different possible configurations of the interface relative to the topography. In this section two cases [(a) and (b)] with an offshore front will be treated, while two other cases [(c) and (d)] will be left for the next section.

However, before dealing with each of the four cases separately, a general expression for the total volume flux Q will first be derived. This applies only to the upper layer; thus using the second and third of (3.5) and the x derivative of the Benoulli function, it follows that

$$\frac{\partial B}{\partial x} \equiv \frac{\partial p}{\partial x} + v\frac{\partial v}{\partial x} = v\left(1 + \frac{\partial v}{\partial x}\right) = Dv. \quad (4.1)$$

Hence the nondimensional volume flux Q in the layer is given by

$$Q = \int Dv dx = B_\infty - B_0, \quad (4.2)$$

where the integration takes place over the x extent of the layer, B_∞ is the value of B at $x = \infty$ and B_0 is the value where the layer depth vanishes. Now at $x = \infty$, $v = 0$ and $p_\infty = D_\infty = 1$, so $B_\infty = 1$ and (4.2) becomes

$$Q = 1 - B_0 = 1 - p_0 - \tfrac{1}{2}v_0^2. \quad (4.3)$$

Case (a)

Here the interface breaks the surface at a point $x = \xi > 0$ where the ocean is infinitely deep. The topography has no effect in this case, the wave speed c is zero (as discussed in the last section) and the equation for ξ is simply

$$\frac{\partial \xi}{\partial t} = 0. \quad (4.4)$$

Case (b)

In this case the front is situated at a point over the shelf region where $x = \xi < 0$. The very deep lower layer with zero potential vorticity has been squeezed onto the shelf, and thus the currents here are no longer negligible. From the nondimensional forms of (2.9), for this layer

$$1 + \frac{\partial v_2}{\partial x} = 0. \quad (4.5)$$

The geostrophic relation is

$$v_2 = \frac{\partial p_2}{\partial x} \quad (4.6)$$

and the hydrostatic equation (2.3) becomes

$$p_1 - p_2 = D. \quad (4.7)$$

Eqs. (4.5) and (4.6) can be integrated immediately using continuity of v_2 and p_2 at $x = 0$ to give

$$v_2 = -x, \quad p_2 = -\tfrac{1}{2}x^2 \quad \text{for} \quad x < 0. \tag{4.8}$$

Substituting in (4.7) and using the geostrophic relation for the upper layer gives

$$p = D - \tfrac{1}{2}x^2, \quad v = \frac{\partial D}{\partial x} - x \quad \text{for} \quad x < 0. \tag{4.9}$$

An equation for D now follows by eliminating v between the second of (3.5) and (4.9), *viz.*,

$$\frac{\partial^2 D}{\partial x^2} = D. \tag{4.10}$$

The solutions which p, D and v are continuous with the solutions given by (3.6) and (3.7) at $x = 0$ is

$$\left.\begin{aligned} D &= \sinh x + \Delta e^{-x} \\ v &= \cosh x - \Delta e^{-x} - x \\ p &= \sinh x + \Delta e^{-x} - \tfrac{1}{2}x^2 \end{aligned}\right\}. \tag{4.11}$$

Furthermore, since D vanishes at $x = \xi$, (4.11) requires that

$$\sinh\xi + \Delta e^{-\xi} = 0, \tag{4.12}$$

which gives the relationship between Δ and ξ. The dynamic condition comes from applying (2.12), i.e.,

$$\frac{\partial v}{\partial t} + v\frac{\partial v}{\partial y} + \frac{\partial p}{\partial y} = 0 \tag{4.13}$$

at $x = \xi$. Substituting from (4.11) and then putting $x = \xi$ (the partial derivatives in (4.13) are derivatives keeping x constant, not keeping ξ constant) gives

$$-\frac{\partial \Delta}{\partial t}e^{-\xi} + \frac{\partial \Delta}{\partial y}e^{-\xi} \times (1 - \cosh\xi + \xi + \Delta e^{-\xi}) = 0. \tag{4.14}$$

Using (4.12) for Δ, this reduces to

$$\frac{\partial \xi}{\partial t} + c\frac{\partial \xi}{\partial y} = 0, \tag{4.15}$$

where

$$c = e^{\xi} - 1 - \xi. \tag{4.16}$$

Thus ξ is constant for an observer moving with speed c given by (4.16). Since ξ is negative c is positive, i.e., waves move the *opposite* way to a normal Kelvin wave (poleward on a western boundary).

Another form of (4.16) is

$$c = v_0 - 1, \tag{4.17}$$

where

$$v_0 = e^{\xi} - \xi \tag{4.18}$$

is by (4.11) the velocity at the point where the layer depth vanishes. The speed v_0 of the current is greater than the wave speed (unity) in the absence of the current, so disturbances are swept in the direction of the stream and *against* the direction they would have in the absence of currents. The flow in this case will be called *supercritical*.

The flux Q of the current can be calculated from (4.3) and (4.11) and using (4.12) to give

$$Q = 1 + \xi e^{\xi} - \tfrac{1}{2}e^{2\xi}. \tag{4.19}$$

Since $\xi < 0$, Q can only have values between 0.5 and 1, with the higher value occurring with the front closer inshore. Q is a function of ξ only, and therefore (4.15) implies

$$\frac{\partial Q}{\partial t} + c\frac{\partial Q}{\partial y} = 0 \tag{4.20}$$

and Q is constant along a *characteristic*, i.e., along a curve defined by

$$\frac{dy}{dt} = c. \tag{4.21}$$

5. Cases where the interface strikes bottom

The remaining two cases shown in Fig. 1 will now be considered.

Case (c)

Here the interface strikes the sloping shelf topography at a point $x = b$, say (where $b < 0$). For $x > b$ the solution is given by (4.11), while at $x = b$ the depth of the upper layer equals the given ocean depth $H(b,y)$. Hence (4.11) gives the following relation between b and Δ:

$$\Delta e^{-b} = H(b,y) - \sinh b. \tag{5.1}$$

Using this in the remaining equations (4.11) gives values of v and p at $x = b$, *viz.*,

$$\left.\begin{aligned} v &= e^{b} - b - H(b,y) \\ p &= H(b,y) - \tfrac{1}{2}b^2 \end{aligned}\right\} \quad \text{at} \quad x = b. \tag{5.2}$$

The potential vorticity equation [second of Eqs. (3.5)] in the region $x < b$ now takes the form

$$1 + \frac{\partial v}{\partial x} = H(x,y) \tag{5.3}$$

and this can be integrated to give

$$v = V(b,x,y) \equiv e^{b} - x - H(b,y) + \int_b^x H(x',y)dx', \tag{5.4}$$

with use being made of the value (5.2) at $x = b$. The function V of b, x and y is defined by (5.4). The way v depends on x, y and t can be determined once b is found as a function of y and t. Similarly, p can be found by integrating the geostrophic re-

lationship [third of Eqs. (3.5)] and using the value (5.2) at $x = b$. The result is

$$p = P(b,x,y)$$
$$\equiv H(b,y) - \tfrac{1}{2}b^2 + \int_b^x V(b,x',y)dx'. \quad (5.5)$$

To find the equation satisfied by b, (2.12) can be applied at the coast $x = w$, where D will be assumed to vanish so that

$$\frac{\partial v}{\partial t} + \frac{\partial B}{\partial y} = 0 \quad \text{at} \quad x = w. \quad (5.6)$$

The derivatives should be calculated from (5.4) and (5.5) *before* putting $x = w$, but it will be shown below that the equation is still true if the order of operations is reversed, i.e., if v and p are evaluated at $x = w$ before (5.6) is applied. We first consider the case where the derivatives are calculated and then x is put equal to w. Use of (5.4) and (5.5) in (5.6) gives

$$\frac{\partial V}{\partial b}\frac{\partial b}{\partial t} + \frac{\partial B}{\partial b}\frac{\partial b}{\partial y} + \frac{\partial B}{\partial y} = 0, \quad (5.7)$$

where

$$B = P + \tfrac{1}{2}V^2. \quad (5.8)$$

If, on the other hand, v and p are first given their values

$$v_0 = V(b,w,y), \quad B_0 = B(b,w,y) \quad (5.9)$$

at the coast (which is also the place where the layer depth vanishes) and the equation

$$\frac{\partial v_0}{\partial t} + \frac{\partial B_0}{\partial y} = 0 \quad (5.10)$$

is applied, the result is

$$\frac{\partial V}{\partial b}\frac{\partial b}{\partial t} + \frac{\partial B}{\partial b}\frac{\partial b}{\partial y} + \frac{\partial B}{\partial x}\frac{\partial w}{\partial y} + \frac{\partial B}{\partial y} = 0. \quad (5.11)$$

This reduces to (5.7) because $\partial B/\partial x$ vanishes at the coast where $D = 0$ by (4.4).

Now since w is a function of y but not of t, (5.9) gives

$$\frac{\partial v_0}{\partial t} = \frac{\partial V}{\partial b}\frac{\partial b}{\partial t}, \quad \frac{\partial B_0}{\partial t} = \frac{\partial B}{\partial b}\frac{\partial b}{\partial t} \quad (5.12)$$

and hence (5.10) may be written

$$\frac{\partial B_0}{\partial t} + c\frac{\partial B_0}{\partial y} = 0, \quad (5.13)$$

where

$$c = \frac{\partial B_0/\partial b}{\partial v_0/\partial b}$$
$$= v_0 + \frac{\partial p_0/\partial b}{\partial v_0/\partial b} = v_0 + w - 1 - b, \quad (5.14)$$

the last expression being obtained when the expressions (5.4) and (5.5) for p and v are used. Using (5.4) again, an alternative is

$$c = \{e^b - 1 - b\} - H(b,y) + \int_b^w H(x',y)dx'. \quad (5.15)$$

The term in braces [cf. Eq. (4.16)] is positive but the remaining terms are negative. When $b = w$, the expression coincides with (4.16), as required, and c is positive. When $b = 0$, the expression in braces vanishes and c is negative. Thus, for some value of b, c vanishes and there is a change from supercritical flow (poleward moving disturbances on the western boundary) to *subcritical* flow, where disturbances move equatorward, i.e., in the same direction as Kelvin waves. (This is then in the direction disturbances travel in the absence of currents.) Note that because of (4.3), Eq. (5.13) is the same equation [(4.20)] as obtained in case (b), i.e., Q is again constant along a characteristic.

There is a consistency condition which must be satisfied if the above expressions are to be valid. This condition is that the slope $\partial D/\partial x$ of the interface just seaward of $x = b$ (see Fig. 1) has to be less than that of the ocean bottom. If (4.11) is used to calculate $\partial D/\partial x$ and (5.1) used to substitute for Δ, the condition becomes

$$e^b < H + \frac{\partial H}{\partial x} \quad \text{at} \quad x = b. \quad (5.16)$$

By (5.4), this is the same as

$$\frac{\partial v_0}{\partial b} < 0. \quad (5.17)$$

If this condition is not satisfied, the interface configuration is not one of the cases shown in Fig. 1, but water from the lower layer on the shelf becomes separated from the rest of the lower layer (which is the region $x > 0$).

Case (d)

Here the interface strikes the vertical cliff at $x = 0$ below the shelf level. As before, if Δ is defined as the interface depth at the shelf edge, it is necessary that

$$\Delta > H(0,y) \quad (5.18)$$

for this case to apply [$H(0,y)$ being the shelf depth at $x = 0$]. The values of v and p at $x = 0$ are given by (3.6) and (3.7), *viz.*,

$$v = 1 - \Delta, \quad p = \Delta. \quad (5.19)$$

The calculations on the shelf are the same as for case (*c*), except for the matching conditions to apply at $x = 0$. Thus, the integral of (5.3) is now

$$v = V(\Delta,x,y) \equiv \Delta + \int_0^x V(\Delta,x',y)dx' \quad (5.20)$$

and the integral of the geostrophic equation [third of Eqs. (3.5)] is

$$p = P(\Delta,x,y) \equiv 1 - \Delta - x + \int_0^x H(x',y)dx'. \quad (5.21)$$

Eq. (4.20) is satisfied as before, i.e., Q is constant along characteristics, and the wave speed [cf. (5.14) and (5.15)] is given by

$$c = v_0 + \frac{\partial p_0/\partial\Delta}{\partial v_0/\partial\Delta} = v_0 + w - 1 = -\Delta + \int_0^w H(x',y)dx'. \quad (5.22)$$

Both terms in the last expression are negative, so $c < 0$ and the flow is *subcritical*. When $w = 0$, (5.22) gives $c = -\Delta$ which reproduces the result of Section 3.

6. Calculations for a shelf with constant slope and variable width

We now consider a special case where the shelf has constant slope s, with the depth H given by

$$H = s(x - w), \quad w < x < 0. \quad (6.1)$$

Then for case (*c*), (5.4) gives

$$v_0 = e^b - w + \tfrac{1}{2}s\{1 - (b + 1 - w)^2\} \quad (6.2)$$

and (5.5) gives

$$p_0 = e^b(w - b) - \tfrac{1}{2}w^2 - \tfrac{1}{3}s\{1 - (b + 1 - w)^3\}. \quad (6.3)$$

The corresponding results for case (*d*) come from (5.20) and (5.21), respectively, i.e.,

$$v_0 = 1 - \Delta - w - \tfrac{1}{2}sw^2, \quad (6.4)$$

$$p_0 = \Delta + (1 - \Delta)w - \tfrac{1}{2}w^2 - \tfrac{1}{3}sw^3. \quad (6.5)$$

These results may then be used to calculate Q using (4.3) and c using (5.14) or (5.22).

Fig. 2 shows contours of c and Fig. 3 shows contours of Q for $s = 1$, chosen because the consistency condition (5.17) is always satisfied if $s \geq 1$. The vertical axis in these figures is

$$W = -w, \quad (6.6)$$

the width of the shelf, while the horizontal axis X is defined by

$$X = \begin{cases} w - \xi & \text{if } w < \xi \text{ [cases (}a\text{) and (}b\text{)]} \\ b - w & \text{if } w < b < 0 \text{ [case (}c\text{)]} \\ \Delta & \text{if } \Delta > -w \text{ [case (}d\text{)].} \end{cases} \quad (6.7)$$

In cases (*a*) and (*b*), $-X$ is the distance of the front (where the interface strikes the surface) from the coast. In case (*c*), X is the distance from the coast where the interface strikes bottom and since $s = 1$, it is also the depth at this point. Similarly for case (*d*), X is the depth of the interface where it abuts the vertical cliff.

The contour $c = 0$ divides the region of supercritical flow ($c > 0$) to the left from the region of subcritical flow ($c < 0$) to the right. The line $c = 0$ is also the line where $\partial Q/\partial x = 0$, i.e., where Q is a *maximum* for a given shelf width W. The region $Q > 0$ is where the flow is poleward on the western boundary (against the direction Kelvin waves propagate), while $Q < 0$ signifies equatorward flow. The curves drawn in Fig. 1 correspond to this example with $W = 1.2$.

To give an idea of magnitude, $\bar{D}$ in the Durban area (see Section 10) has a value of about 300 m for the upper layer of the Agulhas Current, and the corresponding Rossby radius a is about 9 km. The corresponding unit of velocity is about 0.6 m s^{-1} and the unit of transport is $fa^2\bar{D} \approx 1.7 \times 10^6$ m^3 s^{-1}. The shelf slope is about $\frac{1}{60}$, or $\frac{1}{2}$ in nondimensional units.

We now consider some consequences of these results. One property of long waves that can be calculated is the wave steepening effect. Thus consider first the case of an offshore front at $x = \xi$, over the shelf region. The furthest offshore part of a wavy front can be taken as the "crest", and from Fig. 2 since $\partial c/\partial\xi = -\partial c/\partial X$ is negative in the present example, it means that for a shelf of constant width W a trough at a different y will move faster in the positive y direction than the crest. (Note that the volume flux Q at the trough position is also correspondingly greater.) The result is that for this supercritical case, the wave will steepen in the sense shown in Fig. 4a.

In the case where the interface strikes the bottom at $X = b$ the sign of the wave steepening depends on $\partial c/\partial b = \partial c/\partial X$, which is also negative. The wavy front is here defined as the variation in b with y, and the steepening occurs as shown in Fig. 4b. This is the subcritical situation where the wave moves in the opposite direction to the current (i.e., $X > 0$ and $Q > 0$ in Fig. 3) and thus the flux Q at the crest is less than at the trough.

If wave steepening occurs on a surface front, and is not balanced by some other effect such as dispersion, evidence for it could be found from a suitably large sample of surface temperature pictures. If topography is present, deviations from the mean position of the front could indicate the wave steepening. The effect should also show up in (x,t) temperature sections across a front, e.g., in the supercritical case shown in Fig. 4a the interface

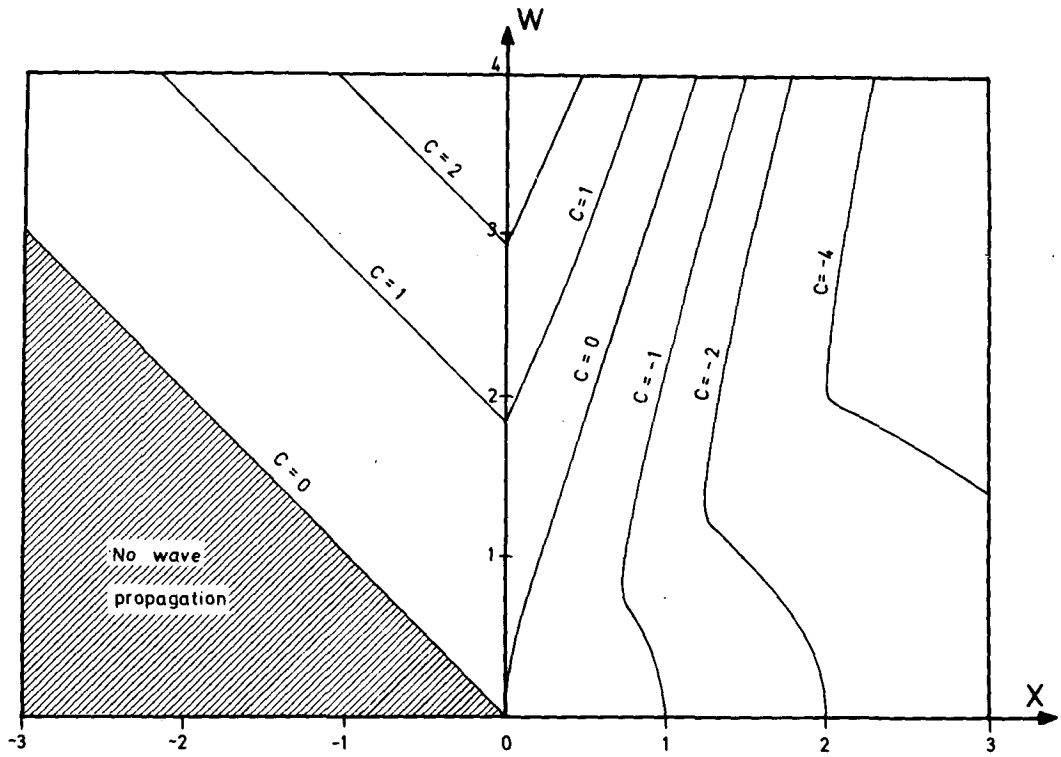

FIG. 2. Contours of the long-wave speed c of disturbances to a uniform potential vorticity current over a shelf of unit nondimensional slope. The vertical axis W is the shelf width and the horizontal coordinate X gives the point where the interface strikes surface or bottom. Positive values correspond to *supercritical* flow, while negative values denote *subcritical* flow. Values are given in nondimensional units.

would tend to move onshore more rapidly than it moves offshore.

In a practical situation both cases would also show up in measurements taken at a level intersecting the front. Such measurements have been made on consecutive days off Durban, and Pearce (1977) depicts a "space-time" map of temperature and salinity with a front steepening in the manner described. Unfortunately, with measurements along a single section, it was not possible to determine the direction of propagation.

Other deductions may be made by analogy with hydraulics problems, and in particular, the flow over a weir. Stommel drew attention to this analogy in his book and results for flows in rotating fluids are discussed by Whitehead *et al.* (1974) and by Gill (1977). For steady flow, Q is constant; thus the dependence of X on W is given by the appropriate contour in Fig. 3. When Q is positive, that is, the current flows in the opposite direction to Kelvin waves, there are two possible values of X for a given W, corresponding to the two cases of subcritical and supercritical flow. In these circumstances, a place where the shelf width is a *minimum* can exert hydraulic control just as a weir does in a nonrotating fluid, and determines the flow upstream of this point. The flow rate corresponding to a particular case where the minimum width is W_{min} can be obtained from Fig. 3, the flow rate being the maximum possible when $W = W_{min}$.

An example of controlled flow in the neighborhood of a control section is shown in Fig. 5. The boundary current is coming poleward along a western boundary toward the reader with a given flux Q of 0.6. Upstream of the control section, the flow is subcritical and the interface strikes bottom on the outer part of the shelf. As the control section is approached, the shoreward edge of the dense water moves toward the coast, and continues to do so beyond the control section where the flow has become supercritical. The dense water then reaches the surface forming a front, and this front maintains its position relative to the shelf break for as long as the flow remains supercritical. It is possible that a hydraulic jump to subcritical flow could occur, with the outcrop of dense water at the surface not occurring downstream of the jump. The form a jump might take in practice is not clear, as there seems no reason to suppose that the potential vorticity distribution downstream of the jump would be the same as it was upstream of the jump. Whether such jumps occur in boundary currents in practice is also not known.

It should be borne in mind that the property of

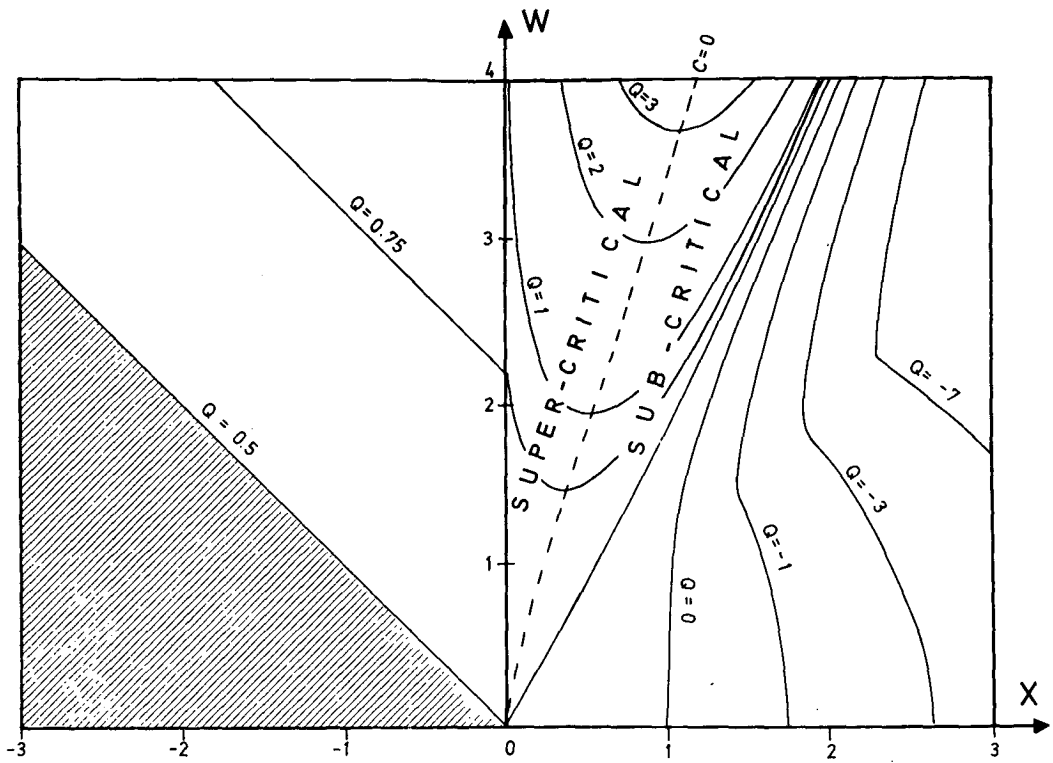

FIG. 3. Contours of the total volume flux Q in the upper layer for the same situation as for Fig. 2. Positive values indicate the flux is in the opposite direction to normal Kelvin wave propagation. Note that the contours have tangents parallel to the X axis on the line where the flow is critical ($c = 0$). Values are given in non-dimensional units.

having transitions from subcritical to supercritical flow at a minimum in shelf width is a property of the particular case studied here. It does not follow that the same is true with boundary currents with different potential vorticity distributions flowing over different types of topography.

The example in Fig. 5, however, does draw attention to one important point—and that is that changes in shelf topography can cause dense water to be brought to the surface along the inner edge of the shelf. This is not a manifestation of "upwelling" in the way this process is usually envisaged, as the motion is mainly horizontal and alongshore. However, individual fluid particles may slowly move upward and shoreward in response to topographic changes and so be forced to the surface without any assistance from the wind or other such agency. In the Agulhas Current system, such dense water is found to outcrop at the surface near to the shore south of 32°S (see, e.g., Bang, 1970), and it seems quite likely that topographic effects of the type discussed here are important factors in causing this to occur. In the above model, outcropping of dense water at the surface only occurs when the flow has become supercritical, but it does not follow that this is necessarily the case for boundary currents with different potential vorticity distributions.

Finally, and despite the words of caution about the applicability of this model to the Agulhas Current, the solution depicted in Fig. 5 does look remarkably like the observed current near Durban. In particular, the reversed flow on the wider shelf to the north of Durban is found, with the above-mentioned upwelling to the south. Later sections describe attempts to model the observed current, at the same time determining whether a transition to supercritical flow can occur where the shelf is narrow.

7. Method of solution for a steady multi-layer jet

The simple model introduced in Section 4 is useful for illustrating the sort of behavior an inertial jet can have when it is influenced by topography, and suggests qualitative features which might be looked for in observations. To apply the ideas in quantitative fashion to a particular current, however, requires much more detailed modeling of the current structure. The example used here to illustrate what may be done is the Agulhas Current in the region shown in Fig. 6. The current flows strongly poleward across this region, and the shelf width decreases considerably in the direction of flow. The model of the previous sections predicts

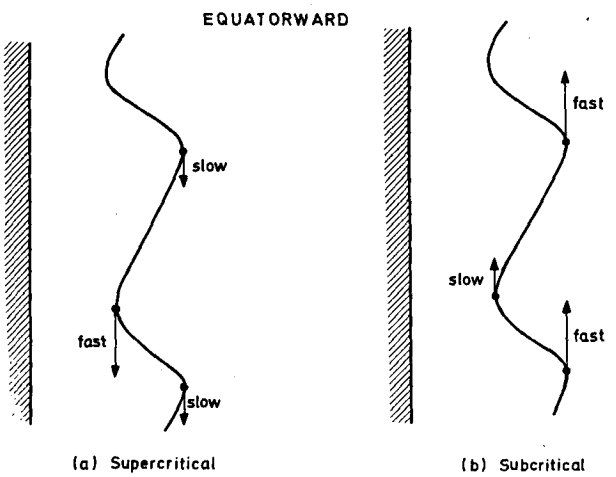

FIG. 4. Wave steepening effects for a uniform potential vorticity current over a shelf of constant slope. (a) Case where the interface strikes the surface. If the line where the interface meets the surface is initially sinusoidal, wave steepening tends to distort it to the configuration shown. This is because crests, that is, points of the front furthest from the shore, tend to move poleward more slowly than the troughs. (b) Case where the interface strikes bottom. In this case the crests, i.e., points on the line of intersection furthest from the shore, tend to move equatorward faster than the troughs.

an intensification of the current in such a region and this, indeed, is found to occur. However, detailed calculations of the changes require a better representation of the way in which potential vorticity and density vary across the section.

The density variations will be modeled by having *two* active upper layers instead of one, and a deep inactive layer off the shelf. It is *not* a good approximation to take a constant potential vorticity in each layer for, as Gill (in Pearce, 1977) pointed out, the potential vorticity in the 16–20°C layer increases by a factor of 3 as one moves toward the shore. A look at the observations shows the high potential vorticities are associated with a region of *cyclonic* vorticity where the current *decreases* from its maximum value toward zero at the coast (which does not happen with the model profiles shown in Fig. 1b). This decrease is presumably a cumulative effect of friction over the whole of the distance in which the current has been rubbing against the shelf, and suggests that a purely inertial theory could not be used to predict changes of current structure over such a large distance. However, in a small distance of the order of 150 km where large topographic changes occur (as in the region of study), inertial effects might be expected to dominate over friction and so a purely inertial theory would be appropriate. Indeed, the calculations by Gill (1977) show that the potential vorticity distribution at the Port Edward section is very similar to that at Durban (see Fig. 6), so the assumption of conservation of potential vorticity over this distance seems justified.

There are two sorts of calculations which will be considered. The first is to calculate how slow geometric changes with distance along the coast induce changes in the current and density structure of a steady flow, assuming potential vorticity is conserved. The second is to calculate the effects of these changes on the speed of long waves, with a view to finding whether there are disturbances which change from being subcritical to supercritical.

In this section, the calculation of the *steady* flow of an inertial jet over topography will be considered. The properties of small disturbances will be treated in a later section. The steady flow can be studied in quite general terms by supposing the current to consist of N homogeneous layers, each having a constant density ρ_i, where $i = 1, 2, \ldots, N$ refers to the number of the layer in order starting at the top. Since the flow is steady, Eq. (2.7) implies that a streamfunction ψ_i can be specified in each layer, where

$$D_i u_i = -\frac{\partial \psi_i}{\partial y}, \quad D_i v_i = \frac{\partial \psi_i}{\partial x}, \tag{7.1}$$

and (2.8) implies that the potential vorticity (2.9) in a given layer is a function only of the stream function for that layer, i.e.,

$$\bar{D}_i = \bar{D}_i(\psi_i), \tag{7.2}$$

where the potential depth $\bar{D}_i$ is a given function of ψ_i.

The way v_i, p_i, D_i and ψ_i vary with x at any given section (y fixed) can be found by solving a set of ordinary differential equations, *viz.*,

$$\frac{\partial v_i}{\partial x} = f\left[\frac{D_i}{\bar{D}(\psi_i)} - 1\right], \tag{7.3}$$

$$\frac{\partial \psi_i}{\partial x} = D_i v_i, \tag{7.4}$$

$$\frac{\partial p_i}{\partial x} = f v_i, \tag{7.5}$$

[which are just rearrangements of Eqs. (2.9) and (7.2), (7.1) and (2.5)] and the hydrostatic equation (2.3). In addition, there is the supplementary condition

$$p_N = 0 \tag{7.6}$$

where the bottom layer (see Section 3) is infinitely deep. Otherwise the condition is simply that the total depth of the layer is equal to the ocean depth H, i.e.,

$$\sum_{i=1}^{N} D_i = H. \tag{7.7}$$

The integration can proceed inward from some large value of x (the method of applying the condition at $x = \infty$ is discussed in Section 8) using standard finite-difference methods (see, e.g., Mour-

sund and Duris, 1967). At certain places, the depth of one of the layers will vanish, and the integration will continue from that point with one less layer. If the convention is adopted that ψ_i is measured from zero at the inner edge of the layer and reaches a value $\psi_{i\infty}$ at $x = \infty$, then, of course, the integration must give $\psi_i = 0$ where the layer depth vanishes. If guessed values are used at infinity to start the integration, the conditions

$$\psi_i = 0, \quad \text{where} \quad D_i = 0 \tag{7.8}$$

will not in general be satisfied, and some interpolation procedure must be used to find the correct starting values.

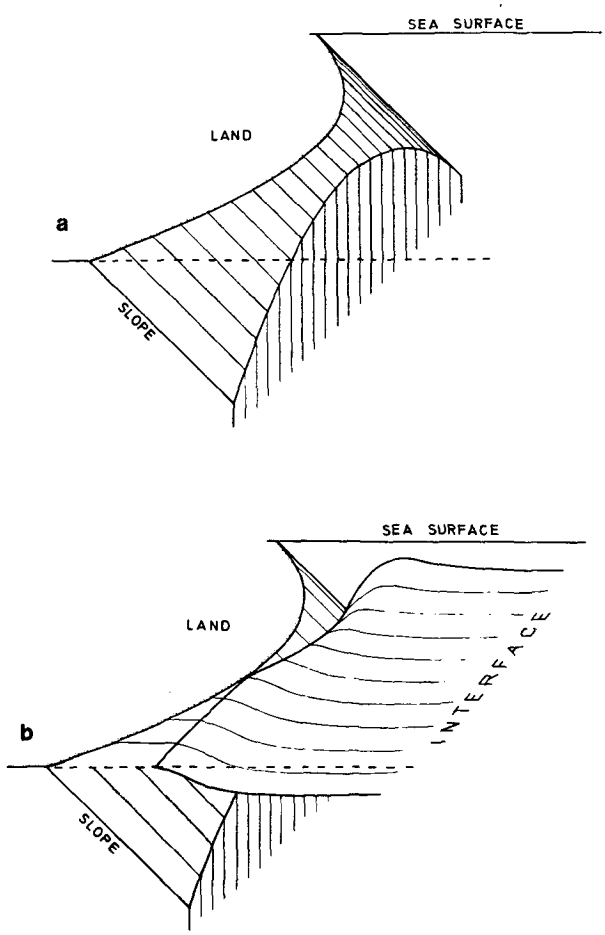

FIG. 5. An example of a boundary current whose flow is hydraulically controlled by the geometry. (a) Topography: The boundary consists of a continental shelf with unit nondimensional slope and a width which varies parabolically with downstream distance. At the shelf break there is a vertical cliff. (b) Configuration of the interface. The current flux in the upper layer is directed toward the reader, with control exerted by the section where the shelf width is a minimum. Upstream of this control section the flow is subcritical with the interface striking bottom on the sloping boundary. The point of intersection rises with distance downstream and reaches the surface a little downstream of the control section. From this point onward, the interface meets the surface in a front which is in a fixed position relative to the shelf break. Shoreward of the front, the cold water of the lower layer outcrops the surface.

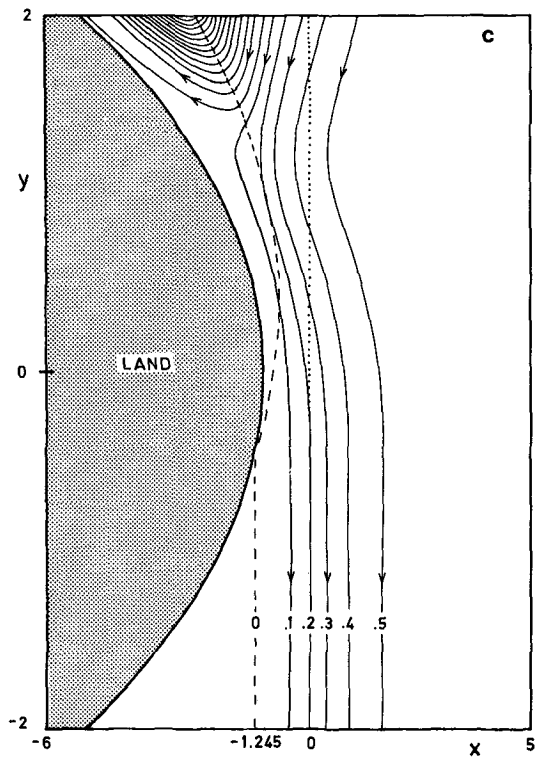

FIG. 5c. Contours of the upper layer streamfunction. The total flux is 0.6, with this value reached as $x \to \infty$; the contour interval is 0.1. Note the flow reversal upstream of the control section.

8. The boundary condition at infinity—expansion in normal modes

Suppose that, at a particular section, the value ψ_i at $x = \infty$ is $\psi_{i\infty}$ and the corresponding value of $\bar{D}_i$ is $\bar{D}_{i\infty}$ given by

$$\bar{D}_{i\infty} = \bar{D}_i(\psi_{i\infty}). \tag{8.1}$$

Then, as $x \to \infty$, the solution satisfies the condition

$$D_i \to \bar{D}_{i\infty}, \quad v_i \to 0, \quad \psi_i \to \psi_{i\infty}, \quad p_i \to p_{i\infty}, \tag{8.2}$$

where the $p_{i\infty}$ can be calculated from (2.3) and the supplementary condition (7.6).

For sufficiently large x, the solution will be a small perturbation from the state given by (8.2) and thus linear theory can be used. As a result the equations to be satisfied are (2.3), (7.5) and the linearized form of (7.3), *viz.*,

$$\frac{\partial v_i}{\partial x} = f\left(\frac{D_i - \bar{D}_{i\infty}}{\bar{D}_{i\infty}}\right). \tag{8.3}$$

The solution representing perturbation from values at infinity can be expressed as a sum of normal modes of the form

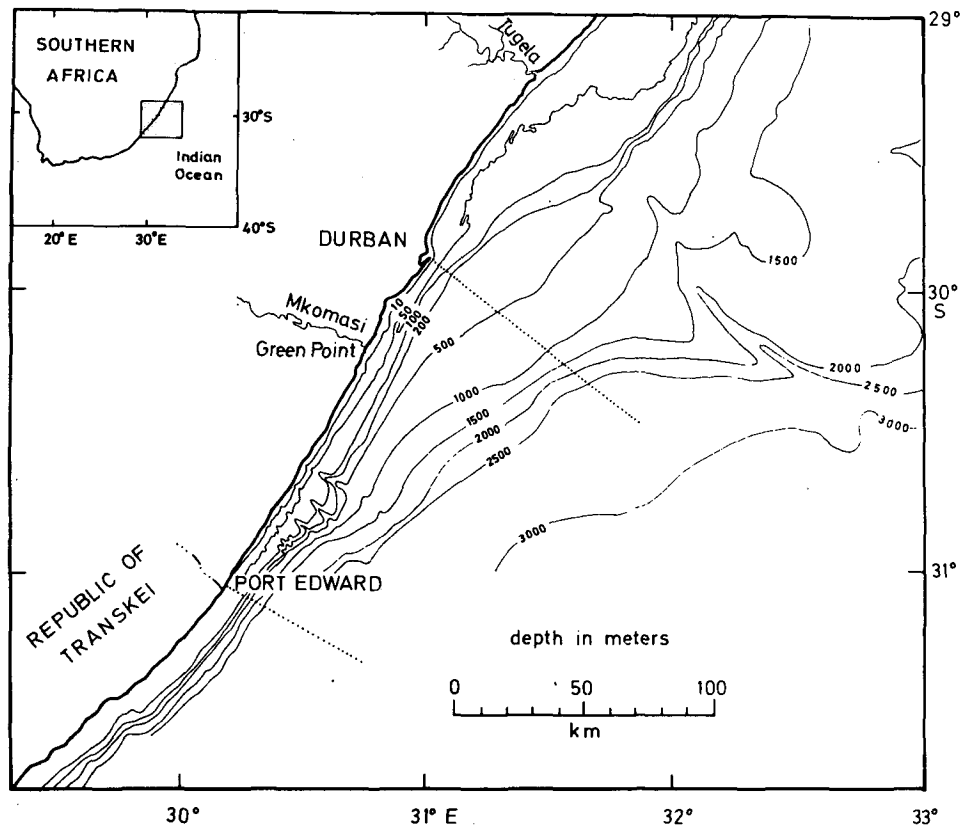

FIG. 6. Bottom topography between Durban and Port Edward after Goodlad (1978) and Moir (1975). The lines along which the sections discussed in the text were measured are also shown.

$$\left.\begin{aligned} D_i - \bar{D}_{i\infty} &= A_i \exp(-\lambda x) \\ v_i &= C_i \exp(-\lambda x) \\ p_i - p_{i\infty} &= C_i' \exp(-\lambda x) \end{aligned}\right\}, \tag{8.4}$$

where by (7.5) and (8.3)

$$C_i = -\frac{fA_i}{\lambda \bar{D}_{i\infty}}, \quad C_i' = \frac{f^2 A_i}{\lambda^2 \bar{D}_{i\infty}}. \tag{8.5}$$

Substitution from (8.4) and (8.5) in (2.3) gives a matrix equation for the vector A_i, *viz.*,

$$f^2\left(\frac{A_{n+1}}{\bar{D}_{n+1,\infty}} - \frac{A_n}{\bar{D}_{n\infty}}\right) = -\lambda^2 g_n \sum_{i=1}^{n} A_i,$$
$$n = 1, 2, \ldots, N-1, \tag{8.6}$$

where by (7.6) and (8.5),

$$A_N = 0. \tag{8.7}$$

The set of homogeneous equations (8.6) has a solution if and only if the determinant vanishes, and this determines the possible eigenvalues $\lambda^{(k)}$ ($k = 1, 2 \ldots N-1$) and eigenfunctions $A_i^{(k)}$ which can be normalized in some way. Thus the condition at infinity can be written

$$\left.\begin{aligned} D_i - \bar{D}_{i\infty} &= \sum_{k=1}^{N-1} b_k A_i^{(k)} \\ v_i &= -\frac{f}{\bar{D}_{i\infty}} \sum_{k=1}^{N-1} \frac{b_k}{\lambda_k} A_i^{(k)} \\ p_i - p_{i\infty} &= \frac{f^2}{\bar{D}_{i\infty}} \sum_{k=1}^{N-1} \frac{b_k}{\lambda_k^2} A_i^{(k)} \end{aligned}\right\}, \tag{8.8}$$

where the b_k ($k = 1, 2 \ldots N-1$) are coefficients which need to be adjusted from some initial guess until the conditions (7.8) are satisfied for each layer.

The only approximation used is to replace $\bar{D}_i$ in (7.3) by $\bar{D}_{i\infty}$, so Eqs. (8.8) can be applied at any x for which $\bar{D}_i$ is close to $\bar{D}_{i\infty}$ for all larger values of x. The value of ψ_i can be found by using the proportionality between changes of streamfunction and changes of Bernoulli function which applies when the potential vorticity is constant [see (4.4) and (7.4)]. This relationship gives

$$\frac{f}{\bar{D}_{i\infty}}(\psi_i - \psi_{i\infty}) = B_i - B_{i\infty} = p_i - p_{i\infty} + \tfrac{1}{2}v_i^2. \tag{8.9}$$

9. The wave speed of disturbances

We now consider small disturbances to the steady flow of the type calculated above. Suppose that the disturbance is *long* compared with the width of the current, so that the boundary-layer assumptions still apply, but is *short* compared with the alongshore (y) scale on which the topography varies, so that the disturbance sees only parallel flow with depth a function of x only. There will be different possible disturbances of this type, each with a different structure and with a different speed c. If a circumflex is used to denote the undisturbed flow, the slightly perturbed flow is assumed to have the form

$$\left.\begin{aligned} v_i &= \hat{v}_i(x) + v_i'(x)\varphi(\gamma) \\ p_i &= \hat{p}_i(x) + p_i'(x)\varphi(\gamma) \\ D_i &= \hat{D}_i(x) + D_i'(x)\varphi(\gamma) \\ u_i &= u_i'(x)\frac{d\varphi}{d\xi}(\gamma) \end{aligned}\right\}, \tag{9.1}$$

where φ is an arbitrary function and

$$\gamma = y - ct. \tag{9.2}$$

Substituting these in (2.3), (2.5), (2.6) and (2.7) yields the following equations for the perturbation:

$$p_{n+1}' - p_n' = -g_n \sum_{i=1}^{n} D_i', \tag{9.3}$$

$$fv_i = \frac{dp_i'}{dx}, \tag{9.4}$$

$$(\hat{v}_i - c)v_i' + \left(f + \frac{d\hat{v}_i}{dx}\right)u_i' + p_i' = 0, \tag{9.5}$$

$$(\hat{v}_i - c)D_i' + \frac{d}{dx}(\hat{D}_i u_i') + \hat{D}_i v_i' = 0. \tag{9.6}$$

An alternative to Eqs. (9.4) to (9.6) can be obtained by first using the expression for u_i' given by (9.5) in (9.6) and then using (9.5) to give v_i' in terms of p_i'. The result may be written

$$\frac{d}{dx}\left(\hat{D}_i \frac{dp_i'}{dx}\right) = f^2 D_i' - \frac{fp_i'}{\hat{v}_i - c}\frac{d\hat{\hat{D}}_i}{dx}, \tag{9.7}$$

where $\hat{\hat{D}}_i(x)$ is the undisturbed value of the "potential depth" (see Section 2), i.e., it is given by [cf. Eq. (2.9)]

$$\frac{1}{\hat{D}_i}\left(f + \frac{d\hat{v}_i}{dx}\right) = \frac{f}{\hat{\hat{D}}_i}. \tag{9.8}$$

The boundary condition of vanishing perturbation as $x \to \infty$ can be used to express the p_i' as sums of normal modes as outlined in the previous section. The relative contributions of each mode can then be found by the requirement that the flux

$$\hat{D}_i u_i' = 0, \quad i = 2, \ldots N - 1, \tag{9.9}$$

at the inshore edge of each layer (whether this be at the coast or at a point where the depth of the layer becomes zero). In terms of p_i', Eqs. (9.5) and (9.4) show that the above condition may be written

$$p_i' + \frac{(\hat{v}_i - c)}{f}\frac{dp_i'}{dx} = 0. \tag{9.10}$$

Finally, the possible values of c are determined by finding under what conditions the flux $\hat{D}_1 u_1'$ in the top layer vanishes at the coast.

10. Application to the Agulhas Current

The region shown in Fig. 6 seems well suited for applying the techniques discussed in previous sections. Thus, while the Agulhas Current flow at any section is approximately parallel to the line of the intermediate depth contours, there are considerable changes in shelf topography over a distance small enough for the conservation of potential vorticity to seem a useful concept. The Current in this region is quite strong, and the geostrophic assumption has been applied with some success to describing the broad flow patterns (Duncan, 1970). In this area the Current sources are the Mozambique Channel [though this is a sporadic source not operating at times (Menaché, 1963)] and a movement of water westward from south of Madagascar and also a recirculation of waters from the south. An inflow into the main current stream south of Durban has also been confirmed by satellite-tracked drifters reported by Stavropoulos and Duncan (1974) and Gründlingh (1977).

The topography off Durban shows a terrace-like structure with the Current core lying some 40–50 km offshore (Pearce, 1977). Although considerable variability in the position of the core is experienced, the Current generally moves closer inshore with the topography in its journey southward. An analysis by Pearce *et al.* (1978) describes a predominantly northward flow close inshore off Durban, and a consequent semipermanent, cyclonic gyre extending to south of Green Point.

The two sections to be used in an application of the model are the ones shown in Fig. 6. Since the currents in practice are not steady, as assumed in the theory, but highly variable, mean sections will be used in the hope that they will be more suitable for applying the theory. The means are based on 42 transects off Durban and 17 off Port Edward which were made in all seasons between 1972 and 1975 (Pearce, 1977). Data were collected on temperature,

salinity and directly measured current velocity to a maximum depth of 500 m. The current was determined by using a hydrosonde lowered from the R.V. *Meiring Naudé* with this reading added on to ship's drift to obtain the absolute current (Stavropoulos, 1971). For present purposes, an average current was computed for the upper 100 m, and with this as a reference level, the geostrophic currents were calculated for the lower 400 m. The average sections of water properties agree well, though the upper waters at Port Edward are slightly less dense.

The two velocity sections thus obtained are shown in Fig. 7. It was decided to simulate these with a three-layer model ($N = 3$) using the $26.2\sigma_t$ surface for the upper interface, and a value $g_1 = 0.019$ m s^{-2}. Fig. 7 shows the positions of the two interfaces and also the layer velocities obtained during the computations. The characteristics obtained from isolated measurements of the deeper waters (M. L. Gründlingh, private communication) indicate an appropriate value for g_2 is 0.008 m s^{-2}.

The equations given in Section 7 were integrated using a fourth-order Runge-Kutta procedure with an integration interval sufficiently small to ensure negligible variation with smaller intervals. Functions $\bar{D}_i(\psi_i)$ were chosen to fit the data shown in Fig. 7. This was done independently for both sections and the results are shown in Fig. 8. It can be seen that there is very good agreement between the sections, showing that the principle of potential vorticity conservation can be used with confidence over such a distance. However, there is a difference between the sections in that the total flux $\psi_{i\infty}$ in each layer is notably greater at Port Edward than at Durban, in keeping with the aforementioned westward moving waters joining the Agulhas Current in this region. This is also in line with the ocean interior flow problem discussed by Greenspan (1969).

Harris and van Foreest (1977) also postulate the existence of a "Mozambique Ridge Current", and that about 10^7 m^3 s^{-1} may join the Agulhas Current from this source south of Durban. In addition, a contribution is likely from the return Agulhas Current; in any case the order of magnitude found here appears to be right.

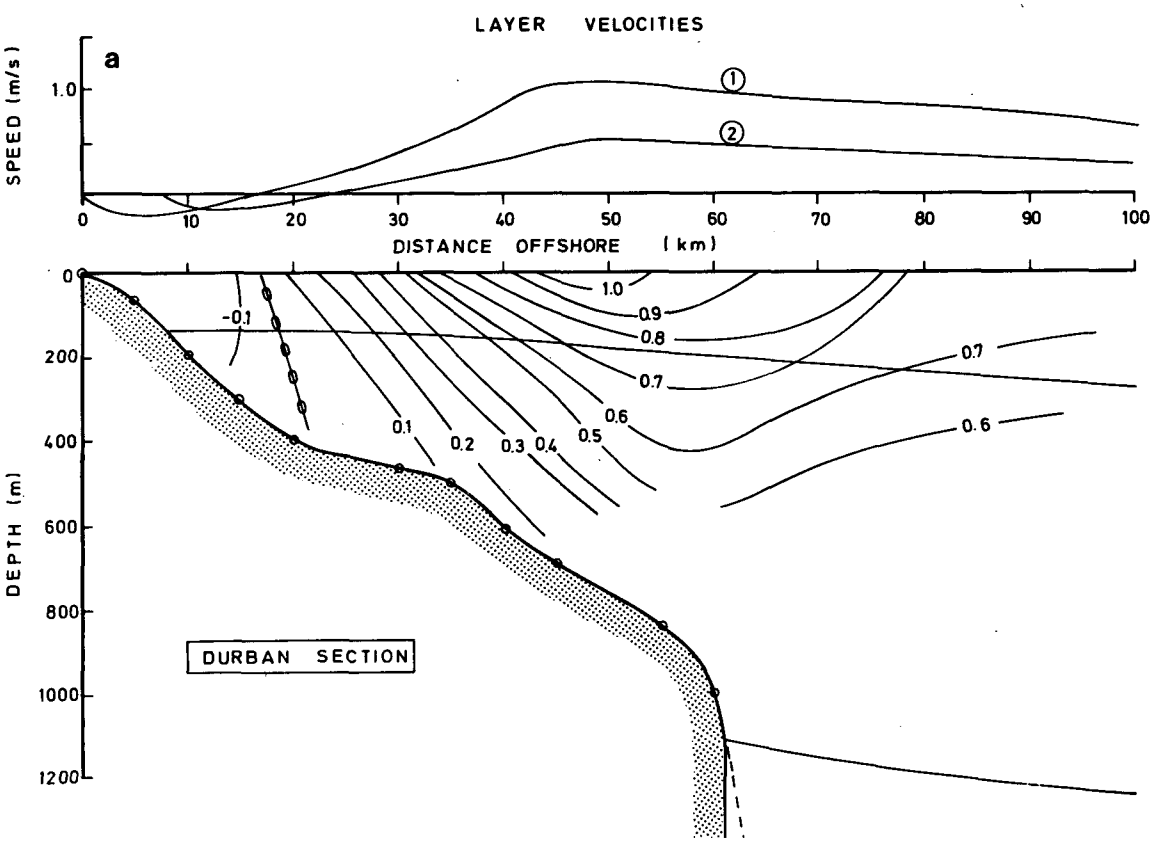

FIG. 7a. The sections off Durban showing contours of longshore velocity obtained by direct measurements using methods outlined in the text. There are also two lines showing the positions of the interfaces used in the model; the upper one corresponds to the $26.2\sigma_t$ isopleth, and does not differ from the measured value by more than 10 m at any point. The upper panels show the layer velocities obtained in the course of the model computations. The bottom topography was modeled by linear sections terminating at the points shown by circles.

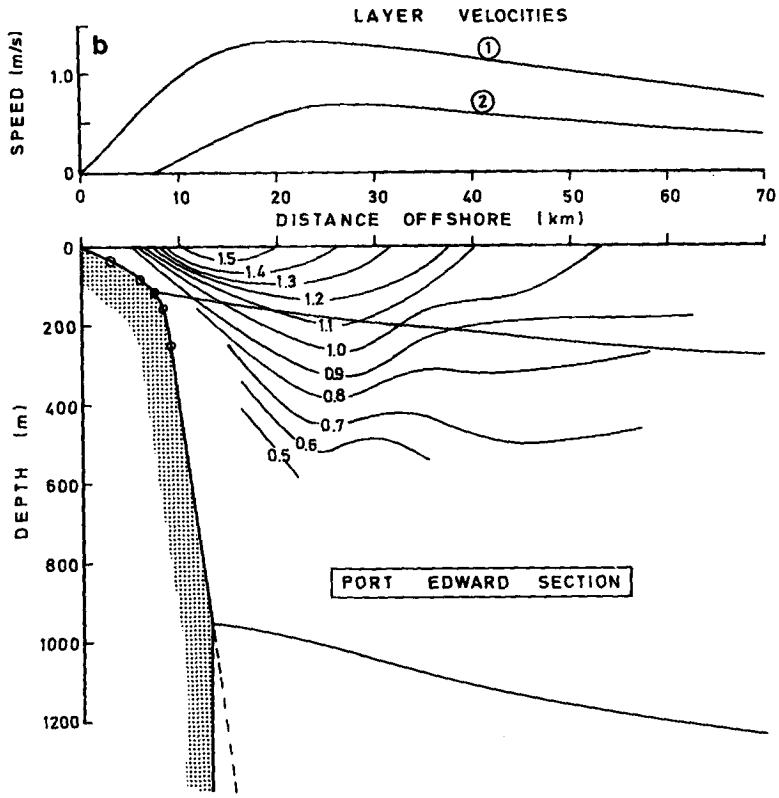

FIG. 7b. As in Fig. 7a except for Port Edward.

This inflow would represent a problem if it were required to calculate the flow at Port Edward using only the inflow data at Durban. This is not sufficient by itself, as the properties of the fluid joining the current from the interior of the ocean need to be known as well. However, it remains true that the method outlined in earlier sections could be used to calculate the current between the two sections on the assumption that the inflow from the ocean interior was evenly distributed between the two sections. Thus the boundary condition as $x \to \infty$ can be such that the $\psi_{i\infty}$ can include given functions of y.

Fig. 8 also shows significant differences in the potential depth in the nearshore region, this presumably being due to friction effects. The region where the differences occur, however, represents only a small fraction of the total flow.

Having modeled the mean flow properties, the wave speeds of long-wave disturbances may then be calculated by the method outlined in Section 9. If there were no shelf (i.e., a vertical cliff at the coast) and no mean current, there would be *two* possible wave speeds. These correspond to the Kelvin-wave speeds which may be determined using the procedure of Section 8. For the values of g_i and $\bar{D}_{i\infty}$ used in the model, these two modes propagate equatorward at speeds of 3.7 and 2.0 m s^{-1}.

If a poleward current (and topography) is introduced, the speeds of the Kelvin modes tend to be reduced, and the amount of reduction can be found by doing the calculation outlined in Section 9. In fact, the final step of this procedure (we are grateful to Dr. Peter Killworth for doing this calculation using a program he has developed for the purpose) was to calculate the value of $\hat{D}_1 u_1'$ at the coast as a function of c, and hence to find by interpolation the values of c for which $\hat{D}_1 u_1'$ vanished. An initial rough calculation showed there are two such values, with the amount of reduction at Port Edward greater than that at Durban. This is in line with the computation from the model studied in Section 6.

Then a more detailed calculation was performed for the Port Edward section using an analytic fit to the velocity profiles shown in Fig. 7b, and approximating the topography by a vertical cliff 10 km from the coast. This gave the first-mode wave speed as 2.4 m s^{-1} and the second-mode speed as 0.4 m s^{-1}. There is, however, some uncertainty in these values because of inaccuracies both in fitting the observations and in the analytic fit. To demonstrate the closeness of the second-mode speed to zero, the velocities were increased until the wavespeed became zero. The increase required was only 15%. It was concluded, therefore, that the second mode at Port Edward was close to being critical and that transition from flow which is second-mode sub-

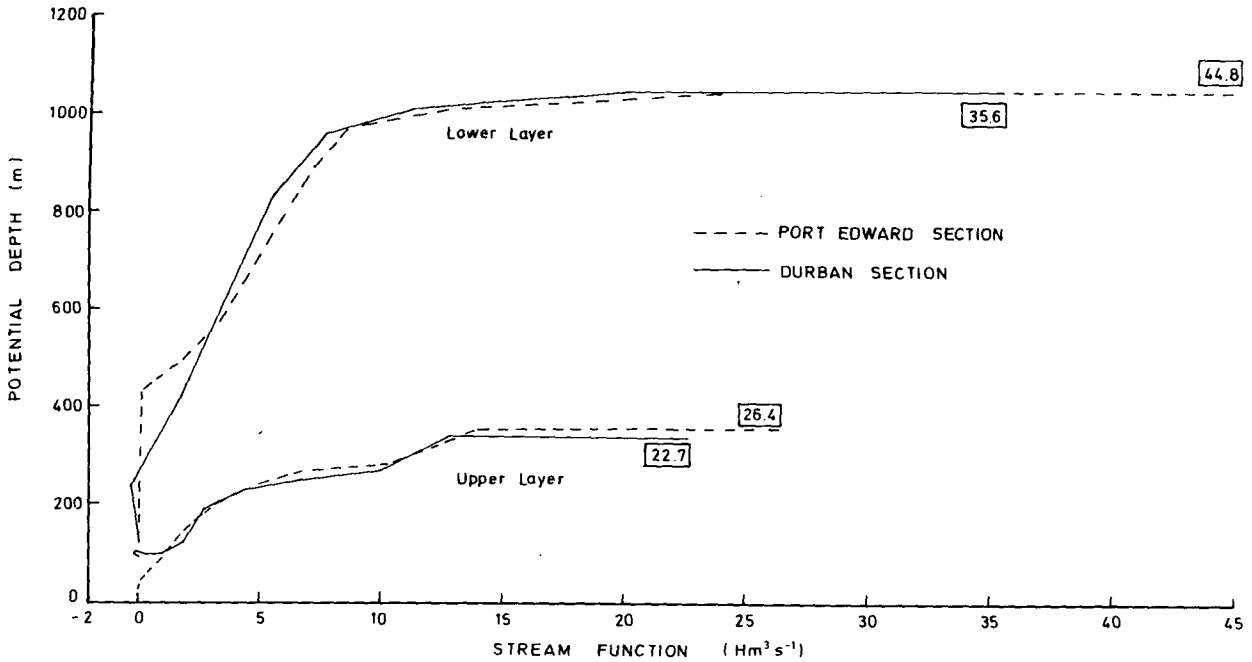

FIG. 8. The potential depth $\bar{D}_i$ as a function of ψ_i obtained in the model simulation for Durban (solid line) and Port Edward (broken line). The figures given at the end of the curves refer to the values of the streamfunction at $x = \infty$.

critical to second-mode supercritical could well occur in the vicinity of Port Edward. Confirmation would require profiles further downstream but these are not available.

It should be mentioned at this point that although the number of modes for layers with *constant* potential vorticity is the same as in the absence of currents, new modes can arise when variable potential vorticity is introduced [this makes the last term in (9.7) nonzero]. Examples are given, for instance, in the review article of LeBlond and Mysak (1977). With the Agulhas current model, only two equatorward-propagating modes were found at each section, and these seem to be the only ones relevant to discussion of transition. It is possible that poleward-propagating modes also exist, but these are not easy to calculate because of the existence of critical layers (i.e., of points where $\hat{v}_i = 0$), and so the calculation was not attempted.

11. Discussion

Where large horizontal gradients occur, it is possible that the simple form of potential vorticity given by (2.9) is no longer conserved. For instance, Hoskins and Bretherton (1972) have used a more complete expression for potential vorticity in their analysis of atmospheric fronts. However, the formulation used here is valid provided that

$$\frac{\partial v}{\partial x}\frac{\partial \rho}{\partial z} \gg \frac{\partial v}{\partial z}\frac{\partial \rho}{\partial x}. \qquad (11.1)$$

Measurements made at the two sections (Durban and Port Edward) indicate that the left-hand side of (11.1) is always at least an order of magnitude greater than the right-hand side, so the formulation used seems appropriate in these circumstances.

Another possible weakness of the simulation is the assumption of no motion below depths of around 1000 m, whereas Duncan (1970) found significant flow at such depths. His estimate of the total transport was in excess of 80×10^6 m^3 s^{-1}, whereas a more recent analysis by Gründlingh (1979) gives $70–80 \times 10^6$ m^3 s^{-1} as a reasonable value, but with large tolerances on any individual measurement. With allowance for the deeper flow, these seem consistent with the estimates obtained here of $60–70 \times 10^6$ m^3 s^{-1} in the two upper layers.

The main interest in the results is the demonstration that changes in shelf topography can cause substantial changes in the structure of a boundary current. In particular, the minimum in the shelf width can exert a hydraulic control on the current, and the example considered in Section 6 showed a tendency for reversed flow upstream of this point and for outcropping of cold water near the shore downstream of this point. Both features are observed with the Agulhas Current near Durban. Computations of the long-wave speed using observed potential vorticity profiles lends support to this idea in that they indicate a transition from flow which is subcritical with respect to the second mode at Durban to flow which is supercritical with respect to this mode downstream at Port Edward.

Acknowledgements. One of us (AEG) would like to express his appreciation to the South African Council for Scientific and Industrial Research for sponsoring a two-month visit to South Africa in 1976, during which time work was started on this paper. We would like to thank Dr. P. D. Killworth for the calculations of wave speeds referred to in Section 10.

REFERENCES

Bang, N. D., 1970: Dynamic interpretations of a detailed surface temperature chart of the Agulhas Current retroflexion and fragmentation area. *S. African Geogr. J.*, **52**, 67–76.

Bennett, J. R., 1973: A theory of large amplitude Kelvin waves. *J. Phys. Oceanogr.*, **3**, 57–60.

Charney, J. G., 1955: The Gulf Stream as an inertial boundary layer. *Proc. U.S. Nat. Acad. Sci.*, **41**, 731–740.

Duncan, C. P., 1970: The Agulhas Current. Ph.D. thesis, University of Hawaii, 76 pp.

Gill, A. E., 1977: The hydraulics of rotating-channel flow. *J. Fluid Mech.*, **80**, 641–671.

Goodlad, S. W., 1978: The bathymetry of the Natal Valley off the Natal and Zululand coasts (Southern Africa). Joint Geological Survey/University of Cape Town Marine Geoscience Group, Tech. Rep. No. 10, 96–104.

Greenspan, H. P., 1969: *The Theory of Rotating Fluids*. Cambridge University Press. 328 pp.

Gründlingh, M. L., 1977: Drift observations from Nimbus 6 satellite tracked-buoys in the south western Indian Ocean. *Deep-Sea Res.*, **24**, 903–913.

——, 1979: The volume transport of the Agulhas Current. Submitted to *Deep-Sea Res.*

Harris, T. F. W., and D. van Foreest, 1977: The Agulhas Current system. Dept. of Oceanography, University of Cape Town, 38 pp.

Hoskins, B. J., and F. P. Bretherton, 1972: Atmospheric frontogenesis models: Mathematical formulation and solution. *J. Atmos. Sci.*, **29**, 11–37.

LeBlond, P. H., and L. A. Mysak, 1977: Trapped coastal waves and their role in shelf dynamics. *The Sea*, Vol. 6, E. D. Goldberg *et al.*, Eds., Wiley-Interscience, 459–495.

Menaché, M., 1963: Premiére campagne océanographique du *Commandant Robert Giraud* dans le canal de Mozambique 11 Octobre–28 Novembre 1957. *Cah. Oceanogr.*, **15**, 224–235.

Moir, G. J., 1975: Bathymetry and hinterland drainage of the Port Elizabeth—Ponto do Ouro continental margin. Marine Geological Unit, University of Cape Town (Chart only).

Morgan, G. W., 1956: On the wind-driven ocean circulation. *Tellus*, **8**, 301–320.

Moursund, D. G., and C. S. Duris, 1967: *Elementary Theory and Application of Numerical Analysis*. McGraw-Hill, 291 pp.

Niiler, P. P., 1975: Variability in western boundary currents. *Proc. Symp. Numerical Models of Ocean Circulation*, Durham, NH, Nat. Acad. Sci., 216–236.

——, and A. R. Robinson, 1967: The theory of free inertial jets II. A numerical experiment for the path of the Gulf Stream. *Tellus*, **19**, 601–619.

Pearce, A. F., 1977: Some features of the upper 500 m of the Agulhas Current. With appendix by A. E. Gill: Potential vorticity as a tracer. *J. Mar. Res.*, **35**, 731–753.

——, E. H. Schumann and G. S. H. Lundie, 1978: Features of the shelf circulation off the Natal coast. *S. African J. Sci.*, **74**, 328–331.

Stavropoulos, C. C., 1971: Data acquisition on the RV *Meiring Naude*. *Electron. Instrum.*, May, 11–15.

——, and C. P. Duncan, 1974: A satellite-tracked buoy in the Agulhas Current. *J. Geophys. Res.*, **79**, 2744–2746.

Stommel, H., 1960: *The Gulf Stream*. University of California Press. 202 pp.

Warren, B. A., 1963: Topographic Influences on the path of the Gulf Stream. *Tellus*, **15**, 167–183.

Whitehead, J. A., A. Leetma and R. A. Knox, 1974: Rotating hydraulics of strait and sill flows. *Geophys. Fluid Dyn.*, **6**, 101–125.